PHYC40970: Advanced Laboratory II

Diffusion-Limited Aggregation

Author: Lainey Ward
Student ID: 18365881
Supervisor: Dr. Nuala Caffrey
November 1, 2021

Abstract

Diffusion-limited aggregation (DLA) is simulated for square and triangular lattices using computational methods. The square lattice model's steplength is revised to reduce the cluster completion time. The color distribution and structure of the clusters are analysed, revealing fractal dimensionalities within a |1.8%| error of theory. The Monte Carlo Method is used to determine the location-dependent growth probability of particle aggregation for a cluster of mass 2. The findings suggest DLA is successfully replicated to a high degree of accuracy.

1 Introduction

Diffusion-limited aggregation (DLA) is the phenomenon in which particles undergoing Brownian motion aggregate irreversibly and form elaborate clusters. The theory of DLA was first developed by physicists Tom Witten and Leo Sander to model colloidal aggregation and has since become widely applicable to many systems. Witten and Sander extensively employed the use of computer simulations to model DLA, as detailed in 'Diffusion-Limited Aggregation, a Kinetic Critical Phenomenon'. Using this basis, a computational model for DLA is devised in Python.

2 Theory

2.1 Diffusion-Limited Aggregation

DLA can be explained in terms of colloidal particles undergoing Brownian motion in a fluid. When a particle is introduced into the system, it can either adhere irreversibly upon contact with another particle, or escape to infinity. The particle density is so low that the aggregation process can be considered to occur one particle at a time. This is the primary foundation upon which Witten and Sander's computational model is formed. DLA applies to the aggregation of any system in which diffusion is the primary mode of transport. [1]

DLA has been most completely studied in two dimensions. However, there are many aspects of the phenomenon that are yet to be understood. Computational developments over the past 40 years have enabled DLA to flourish as an ongoing field of research.

2.2 Fractal Patterns

The aggregation clusters captured by this process share some general features. Their structures tend to be both highly fractal and branched.

The fractal structure arises as the exposed branches overshadow the inner fjords, making them less-accessible. Therefore, the probability of growth declines as a walker progresses down a fjord. This leads to lower growth probabilities at radii near the seed particle than at radii near the tips of the cluster.

The fractal dimension (D) connects the mass of the cluster (M) with its radius (R). In two dimensions, D is approximately 1.71, and 2.5 in three dimensions. For a spatial dimension d greater than 3, the value of D is equal to $d - 1$.

fractal dimension is also sensitive to the lattice structure, cluster mass and system geometry in question. For a DLA model with either a square lattice or no underlying structure or for a square, D is 1.71. For a square lattice with high mass, this value can become approximately 1.5. For radial growth from a seed D remains a value of 1.71. However, for growth from a surface or channel, D can decrease to 1.67. Regardless, D is always ≥ 1.5 in two dimensions. [2]

In the case of the square lattice, assuming the cluster grows radially and does not exceed a mass of 6000 particles, D can be taken to be 1.71.

The cluster mass inside a circle of radius R is:

$$M(R) = kR^D \tag{1}$$

with k, some parameter.

Rearranging this equation returns the the dimensionality of a fractal in terms of its radius and mass:

$$D = \frac{\ln M}{\ln R} \tag{2}$$

R is measured in lattice constants (lc) and D is unitless.

2.3 Applications

Aside from computational models, DLA patterns arise naturally in the real-world. For example, DLA influences the formation of frost patterns on a windshield, the occurrence of Lichtenberg figures on the skin of lightning-strike victims, the growth of coral and crystals. [2] [3] [4]

Recent developments in the theory of DLA have also led to its application across many industries. For example, DLA has been used to predict the evolution of river networks, to recover oil deposits, and has even been incorporated into string theory. [2]

3 Computational Methods

3.1 Model Basis

Section 2.1 is adapted to form the basis of the computational model. A seed particle is positioned at the centre of a square lattice. A second particle or 'walker' is added at a random site at a set radius from the origin. The particle can move in one of four directions randomly in single-step increments until it occupies a site adjacent to the seed, following which it sticks irreversible and joins the aggregation cluster. Another particle is added at a random radius again and it walks until it joins the two-particle cluster, and so on.

If a particle touches the lattice boundary then it is discarded and a new particle is regenerated as before.

In the model, four main processes are considered in which:

- the initial state of the system is initialised.
- the particles are regenerated.
- the random walk is conducted.
- the locational properties are tracked i.e. is the particle near a boundary or beside another particle?).

It is convenient to combine the third and fourth point into one process. Three functions are devised to focus on each process. In accordance with the attached Python scripts, these functions are referred to as DLAMain, RandomLocation and CheckLocation, respectively.

3.2 Model Dimensions

The computational mode is constructed to have only one input variable: the radius of the regeneration circle. All other dimensional terms emerge from this value.

The dimension of the square lattice is $2R+5$. The $+4$ constant allows for a padding spacing of 2 between the left, right, top and bottom x- and y-maxima of the circle and the square lattice. This ensures that when walkers leave these points on the circle boundary, their location does not immediately coincide with the lattice edge.

For simplicity, the x and y coordinates of the seed particle are positioned at $R + 2$. These dimensions are depicted in Fig. 1a. The position of the walker in the upper-right hand corner is relevant to the variation of step length in Section 3.6.

3.3 Model Matrix

A matrix is established according to the dimensions discussed in the previous section. Each element of the matrix corresponds to each possible particle location within the square lattice. In this way, the locations of the elements of the physical system (lattice, circle and particles) can be expressed as a matrix. Fig. 1b depicts such a system overlaid by its corresponding matrix.

In the DLAMain function, the matrix is initialised with values 0, 1 and 2. 0 corresponds to an unoccupied location - one in which there are no aggregated cluster particles. 1 corresponds to an occupied location. 2 corresponds to a location outside of the regeneration circle boundary.

It is apparent in Fig. 1b that at low radii, the circle appear in 'low resolution'. There is a large discrepancy between the input radius (R_{set}) and the actual radius R_{comp} of a particle on the circle boundary. For example, in Fig. 1b $R_{set} = 5$ whereas R_{comp} can range from $4.2 - 5$ lc. It is anticipated that the relative difference between R_{set} and R_{comp} is less appreciable for greater value of R_{ste}.

3.4 Combined Model

Within the CheckLocation and DLAMain functions, there are four ongoing Boolean values representing the occupancy of neighbours, being outside of the circle perimeter, being near the square perimeter and for the completion of the cluster.

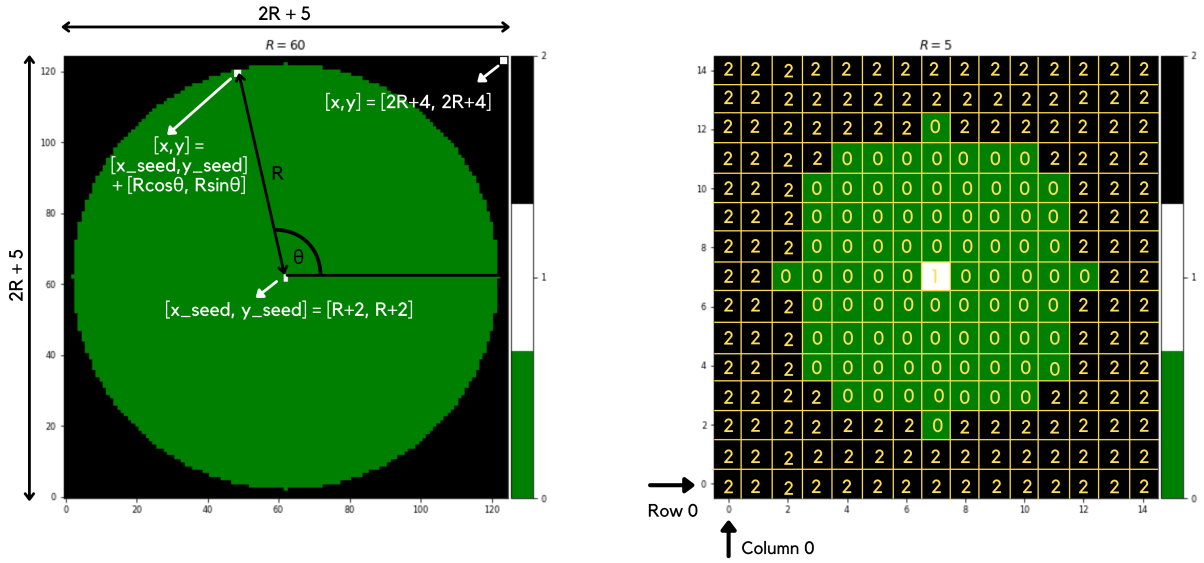

(a) Circle of radius 60 annotated with dimensional details.

(b) Circle of radius 5 annotated with corresponding matrix.

Fig. 1: DLA heatmap of a square lattice of $sl = 1$ with a single seed particle.

If a walker has an occupied neighbour and a neighbour outside of the circle i.e two neighbours having values of 1 and 2, then this implies that the cluster has reached the regeneration circle boundary and is complete.

The perimeters of the square correspond to all values along column 0, row 0, column 14 and row 14 of Fig. 1b. If one of a walker's neighbouring locations coincides with this perimeter, then the movement of the walker is considered unsafe. The walker is discarded and a new random walker is regenerated on the circle perimeter by calling the RandomLocation function.

In the DLAMain function, a count is also kept of the total number of walkers and the number of aggregated walkers. A timer is also ran from the moment of the addition of the first walker until the completion of the cluster. This function also stops the aggregation process if the maximum number of total walkers exceeds 10000. This is good practice as it prevents the repetition of infinite iterations in the case of a looping error occurring within the code.

3.5 Triangular Lattice ($ls = 1$)

The computational model for a triangular lattice follows the same theory as the square lattice in Section 3.1-3.4, but requires some modifications.

The CheckLocation function remains unchanged. The method for particle generation is entirely revised in the RandomLocation function and a minor modification is made to the method for system initialisation in the DLAMain function.

Furthermore, in the context of the triangular lattice, the radius represents the distance from the centre of mass of the triangle to any of its vertices. The dimensions of the square matrix is $2R + a$ and the centre of the triangle is positioned at coordinates $(R, R - b)$, as shown in Fig. 2a. a and b are constants that centre the triangle when plotting.

Using the radius and the centre point, the location of the three vertices can be determined using trigonometry. In the RandomLocation function, these points are used to construct three linear functions between each vertex. An x coordinate is generated randomly along each linear function, following which one is randomly selected. The corresponding y coordinate is calculated using the x coordinate and its paired linear function.

In the MainDLA function, the three vertex locations are converted to barycentric coordinates α, β and γ. A point lies within the triangle if If all three coordinates are ≥ 0.[5] This method is used to initialise the values of 2 in the matrix. The rest of the MainDLA function remains unchanged.

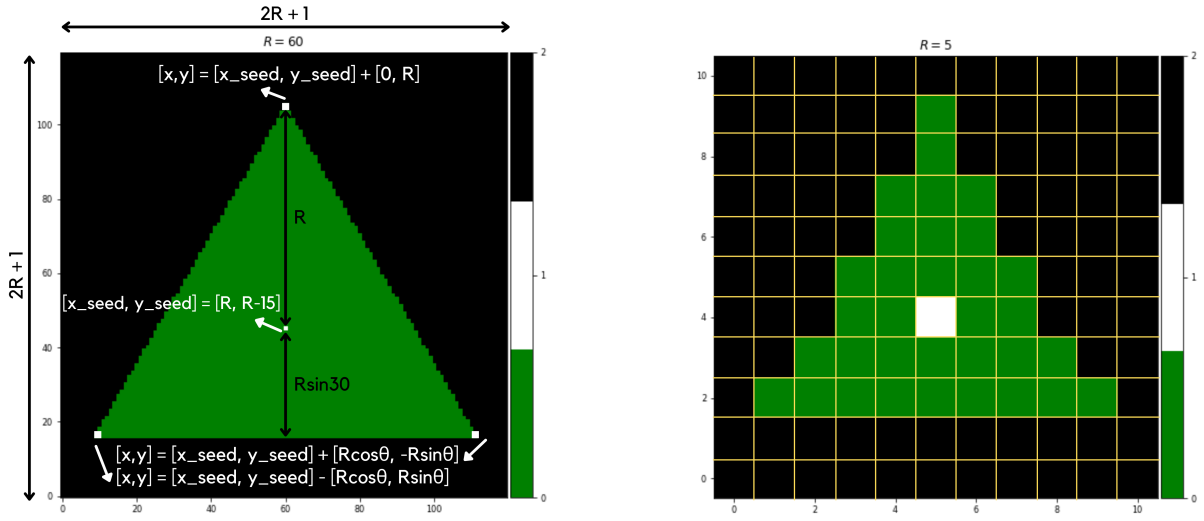

(a) Triangle of radius 60 annotated with dimensional details.

(b) Triangle of radius 5 annotated with its corresponding matrix partition.

Fig. 2: DLA heatmap of a triangular lattice of $sl = 1$ with a single seed particle.

3.6 Square Lattice ($sl \geq 1$)

The computational model for the square lattice for $ls = 1$ is modified to enable the step length (sl) to increase outside of the circle, and remain 1 within the circle.

The first modification takes place in the MainDLA function. It is checked that the current distance from the walker to the seed is greater than the circle. In this case, the step length is taken to be $R_{comp} - R_{set}$. In the case where the R_{comp} is less than or equal to R_{set}, then the steplength remains 1.

For example, for $R_{set} = 30$, if the particle is at a radius of 29,30 or 31, the step length remains 1, but at a distance of 32, 33 or 34, the step length becomes 2, 3 and 4.

The second modification occurs in CheckLocation function. As before, it is checked that a move equal to the newly defined step length will take the runner to the edge of the square. The adjacent locations at a distance of $ls = 1$ are also checked for occupancy. In the case of no occupancy, the walker is permitted to move with its newly determined steplength. The occupancy of this farther position does not have to be checked, as the aggregate does not form outside of the circle.

4 Results & Analysis

In Section 4.1, the model of the square lattice with a steplength of 1 is analysed. In Section 4.2, the models of the square lattice with a steplength ≥ 1 and the triangular lattice are analysed. Finally, in Section 4.3 a Monte Carlo simulation is run for the model of the square lattice with a steplength of 1 to determine the growth probabilities of a cluster of mass 2.

4.1 Square Lattice ($sl = 1$)

The DLA model is run for varying values of R_{set}. Fig. 3 shows a typical configuration of a fractal pattern within the set circle and square. It is apparent from the rightmost white aggregate point that the cluster reaches completion upon contact with the circle edge.

Heatmaps are produced for four different values of R_{set} in Fig. 10. As discussed in Section 2.2, the produced patterns are highly fractal and branched. The difference in growth probabilities between the cluster tips and fjords is especially apparent in the figure for $R_{set} = 100\ lc$. The red colour indicates the most newly added particles and so lack of red seen within the fjords implies that there is a low growth probability at low radii.

It is also checked that the model returns a value

of R_{comp} in close proximity to R_{set}. It is apparent that this is the case in Fig. 4, in which the theoretical model of slope 1 lies within the 95% confidence interval of the data model. For values of $R_{set} < 60$, the model has an increased tendency to underestimate R_{comp}. This can be attributed to the discrete geometry of the model at low values of R_{set}, as discussed in Section 3.

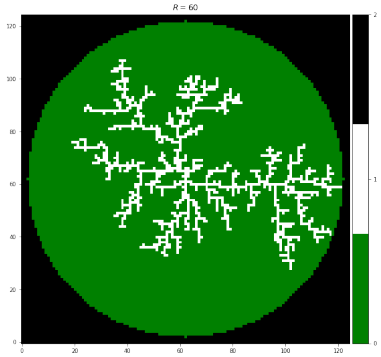

Fig. 3: DLA heatmap depicting a complete cluster.

A log-log plot of R_{comp} against M is produced in Fig. 5 for values of R_{set} in the range of $20 - 140\ lc$. The data is fitted to an ODR with the estimated parameters:

$$ln(R_{set}) = (1.703 \pm 0.006)\, ln(M) \tag{3}$$

According to Eq. 2, the fractal dimension can be taken as (1.703 ± 0.006). This corresponds to a low percent error of -0.38% with respect to the theoretical value of 1.71. The fitting parameter also has a low relative error of 0.4%.

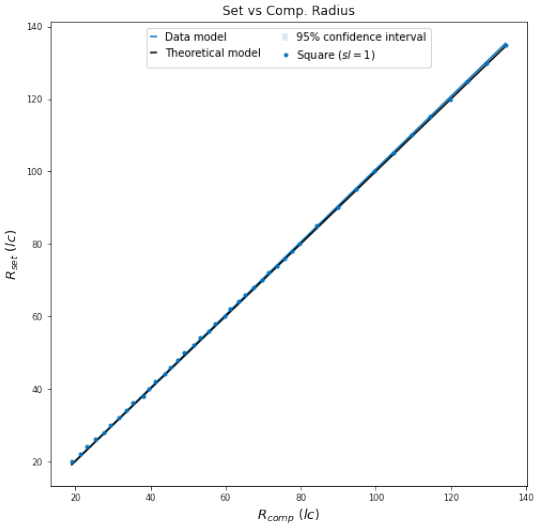

Fig. 4: Data obtained for a square lattice of $sl = 1$ for varying circle radii.

There is a significant, strong correlation ($r =$

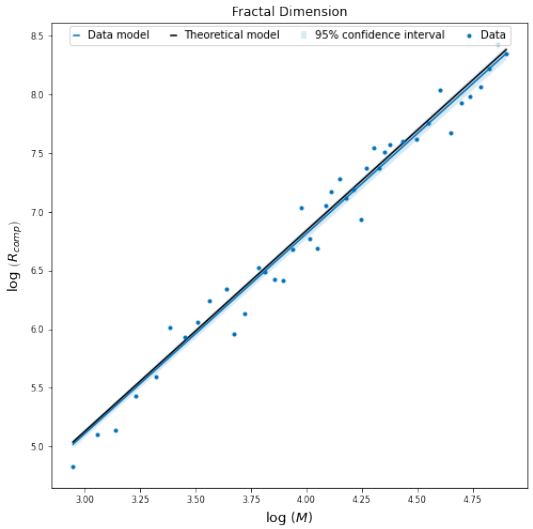

Fig. 5: Data obtained for a square lattice of $ls = 1$ for varying circle radii.

.987, $p < .0001$) between the variables. A Chi-squared statistic test is performed for the null hypothesis that there is no statistical difference between the data and theoretical models. The Chi-squared statistic (χ^2) is greater than the critical value ($\chi_c{}^2$) and so the null hypothesis is rejected. For references, r, p and χ^2 figures are listed in Table 1.

Furthermore, the theoretical model lies within the 95% confidence interval of the data model. Overall, it can be concluded that the data model closely coincides with that predicted by theory.

4.2 Square Lattice ($sl \geq 1$) & Triangular Lattice ($sl = 1$)

Section 4.1 is repeated for a square lattice of $sl \geq 1$ and a triangular lattice of $sl = 1$. Heatmaps are produced for four different values of R_{set} in Fig. 11 and 12. These appear similar in nature to that of Fig. 10. There appear to be no distinguishing features between the heatmaps.

A log-log plot of R_{set} against M is produced again for all three models in Fig. 6. Corresponding data and analysis are given in Table. 1.

Model	D	%	r	p	$\chi^2 \geq \chi_c{}^2$
Square ($sl = 1$)	1.703±0.006	-0.38	.987	$< .0001$	✓
Square ($sl \geq 1$)	1.689±0.013	-1.21	.990	$< .0001$	✓
Triangle ($sl = 1$)	1.740±0.011	1.75	.967	$< .0001$	✓

Table 1: Data obtained from from Fig. 6 for varying set circle and triangular lattice radii.

All three models produced a fractal dimension

within a ±1.8% error from the theoretical value of 1.71, have a strong significant correlation and can reject the null hypothesis of statistical difference between the data and theoretical models. The triangular-lattice model produces the greatest percent error, lowest correlation and lowest significance value of the three models. The theoretical model also lies just outside its 95% confidence interval.

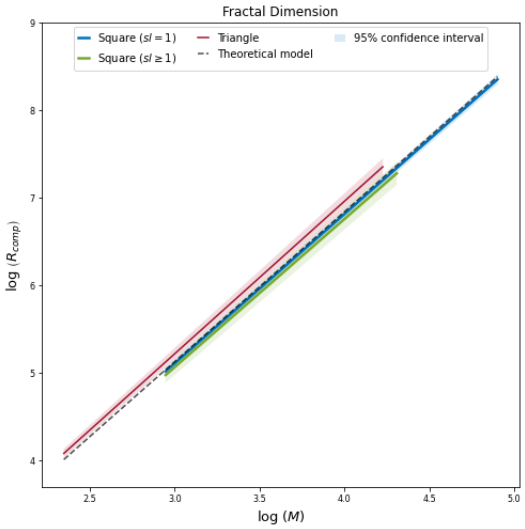

Fig. 6: Data obtained for a square lattice of $ls = 1$ and $ls \geq 1$, and a triangular lattice of $ls = 1$ for varying radii. The theoretical model represents the case for which $D = 1.71$.

R_{comp} is plotted against the DLA fail rate in Fig. 7 and 8. The fail rate is taken as the ratio of unsuccessful walkers to the total number of walkers. The corresponding fitting data is given in Table. 2.

Model	r	p
Square ($sl = 1$)	.810	$< .0001$
Square ($sl \geq 1$)	.834	.001
Triangle ($sl = 1$)	-.043	.793

Table 2: Data obtained from Fig. 7 and 8.

The model for $sl \geq 1$ has a consistently higher fail rate than that for $sl = 1$. It could be interpreted that the increased steplength outside the circle of the $ls \geq 1$ model prompts walkers to leave the square edge at a quicker rate, as opposed to returning to the circle. This would be expressed in a decrease in the cluster completion time, and an increase in the fail rate.

However, in Fig. 7 a log-log plot of R_{comp} against T is produced. This plot suggests that for a given R_{set}, the $ls = 1$ model attains a lower completion time than the $ls \geq 1$ model. Therefore, the increased steplength is not prompting a quicker rate of completion, as anticipated.

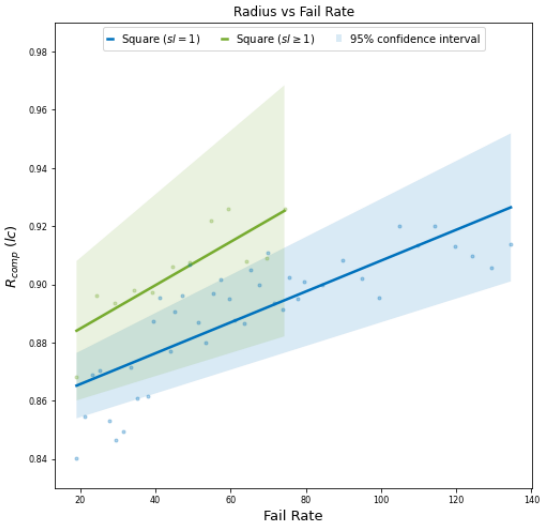

Fig. 7: Data obtained for a square lattice of $ls = 1$ and $ls \geq 1$ for varying circle radii.

Overall, the reasoning for the combination of a higher fail rate and a higher completion time for the $ls \geq 1$ model remains inconclusive.

Furthermore, Fig. 8 shows a low, insignificant correlation between R_{comp} and the fail rate for the triangular lattice model. This implies that as the triangle radius increases, the walkers are not necessarily more likely to leave the triangle edge and not return.

In Fig. 7 it is apparent that the triangular-lattice model attains the lowest completion time of the three models. This is because the nearest point on the triangle edge is $Rsin30$, as opposed to R, in the case of the square lattice. Ideally, this model should be reconfigured so that the $Rsin30$ distance is equals R instead.

Model	r	p
Square (sl= 1)	.999	$< .0001$
Square (sl≥ 1)	.999	$< .0001$
Triangle (sl= 1)	.993	$< .0001$

Table 3: Data obtained from Fig. 9.

Overall, Table 3 shows a high, significant correlation between R_{comp} and T for all three models.

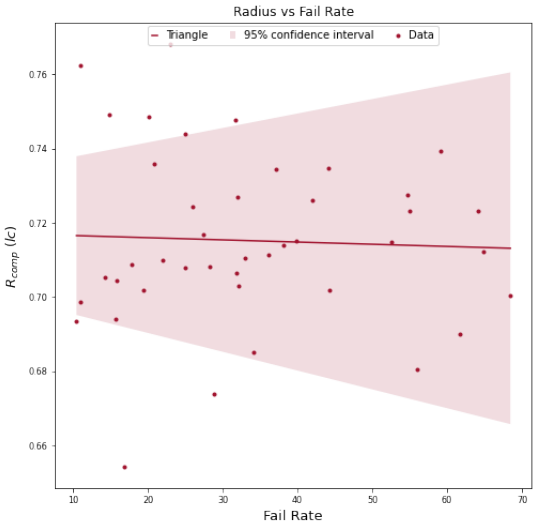

Fig. 8: Data obtained for a square lattice of $ls = 1$ and $ls \geq 1$ for varying circle radii.

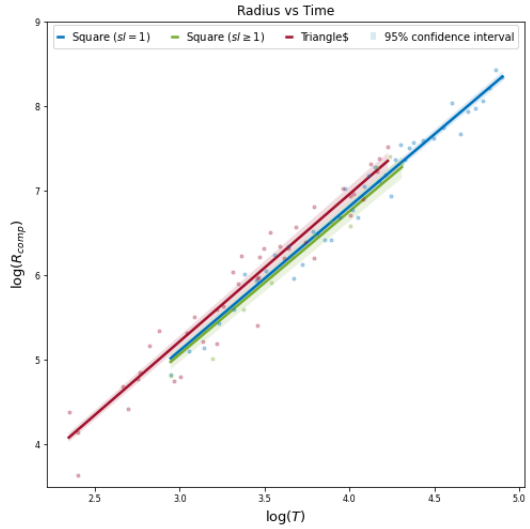

Fig. 9: Data obtained for a square lattice of $ls = 1$ and $ls \geq 1$, and a triangular lattice of $ls = 1$ for varying radii.

4.3 Monte Carlo Square Lattice ($sl = 1$)

The Monte Carlo simulation is run for varying numbers of iterations (N_T) and set radii. The probability of the runner aggregating (N_{AG}) to one of the six possible locations is expressed with respect to the number of total iterations:

$$p_i = \frac{N_{AG}}{N_T} \tag{4}$$

with i, the location number.

Table. 4 gives the values of N_T, R_{set} and p_{1-6} obtained for the Monte Carlo simulation. The coefficient of determination (r_2) is also given in Table. 5, with respect to the corresponding theoretical p_{1-6} values shown in bold.

N_T	R_{set}	mp_1	p_2	p_3	p_4	p_5	p_6
-	-	**0.222**	**0.222**	**0.139**	**0.139**	**0.139**	**0.139**
3000	10	0.219	0.229	0.145	0.158	0.100	0.149
100000	10	0.201	0.226	0.147	0.155	0.133	0.139
100000	40	0.211	0.216	0.141	0.143	0.145	0.145
36000	40	0.207	0.217	0.139	0.144	0.145	0.149
10000	80	0.215	0.214	0.137	0.145	0.144	0.144

Table 4: Data obtained for a Monte Carlo simulation of a square lattice DLA system with a seed particle and 2 runners.

N_T	R_{set}	r_2
-	-	**1.000**
3000	10	0.774
100000	10	0.911
100000	40	0.972
36000	40	0.956
10000	80	0.978

Table 5: Regression data obtained for data from Table. 4.

In theory, the coefficient of determination of the set of location probabilities should equal 1 with respect to itself. Firstly, for $R_{set} = 10$, r_2 significantly increases from $\sim 0.77 - 0.91$ for an increase of N_T from 3000 to 100000. The same is apparent for an increase in R_T from $36000 - 100000$ for $R_{set} = 40$. Therefore, for a given set radius, r_2 is in closer proximity to theory for increasing values of N_T.

Secondly, for $N_T = 100000$, r_2 slightly increases from $\sim 0.91 - 0.97$ for an increase in R_{set} from $10 - 40$. Overall, this suggest that the Monte Carlo probabilities approach their corresponding theoretical values as N_T and R_{set} approach infinity.

However, it is worth noting that the highest r_2 value is attributed to a low N_T value of 10000 and a high R_{set} value of 80. This may indicate that the circle radius takes greater precedence than the number of iterations in attaining an r_2 value of 1. This theory requires more sets of data than that given in Table. 4 to be confirmed.

5 Conclusion

Computational models for diffusion-limited aggregation are devised and analysed for square and triangular lattices. The former is analysed for both a steplength of 1 and a steplength ≥ 1 outside of the circle boundary. The latter is analysed for a steplength of 1 only.

It is found that clusters formed by the square lattice models successfully attain a radius significantly equal to the radius of the circle, as anticipated.

Heatmaps are produced for all three models at 4 different radii and present highly branched, fractal structures. Their color distribution indicates that the exposed tips of the clusters have a higher growth probabilities than the sheltered fjords.

The fractal dimension is determined from a log-log plot of the circle radius against the cluster mass. Using regression analysis, the fractal dimension of the square lattice for $sl = 1$ is within a $|0.4\%|$ error of theory. The two other models also lie within a $|1.8\%|$ error. Using a Chi-Squared test, it is concluded that there is no significant difference between the three data models and the theoretical model.

A strong, positive correlation is found between fail rate, circle radius and completion time for the square lattice. Unexpectedly, the model for $sl \geq 1$ has a greater walker fail rate and a longer completion time than the square lattice model for $sl = 1$. The two-primary modifications made to the $sl = 1$ model require further analysis to confidently comprehend and account for this disparity.

Finally, a Monte Carlo simulation is undertaken for varying values of circle radius and iteration number for a cluster of mass 2. It is found that the that probability of aggregation for the six locations approach their corresponding theoretical values with increasing circle radius and iteration number. The results also suggest that the radius takes greater precedence than the iteration number in attaining probabilities closest to theory.

In conclusion, the computational models devised successfully replicate the real-world phenomenon of diffusion-limited aggregation to a high degree of accuracy.

References

[1] T. Witten and L. Sander, "Diffusion-limited aggregation, a kinetic phenomenon," *The American Physical Society*, vol. 47, no. 19, pp. 1400–1403, 1981.

[2] T. Halsey, "Diffusion-limited aggregation: A model for pattern formation," *Physics Today*, vol. 53, no. 1, pp. 36–41, 2020. DOI: 10.1063/1.1333284.

[3] S. Nigrelli *et al.*, "A finite-volume diffusion-limited aggregation model for predicting the effective thermal conductivity of frost," *International Journal of Heat and Mass Transfer*, vol. 101, no. 1, p. 1263, 2016. DOI: 10.1088/1742-6596/891/1/012052.

[4] S. Wang *et al.*, "Growth diffusion-limited aggregation for basin fractal river network evolution model," *AIP Advances*, vol. 10, no. 1, pp. 1400–1403, 2020. DOI: 10.1063/5.0011624.

[5] U. Berkley, "Lecture 5: Texture mapping," 2020. url: https://cs184.eecs.berkeley.edu/sp19/lecture/5-21/texture-mapping.

6 Appendix

6.1 Additional Figures

PTO

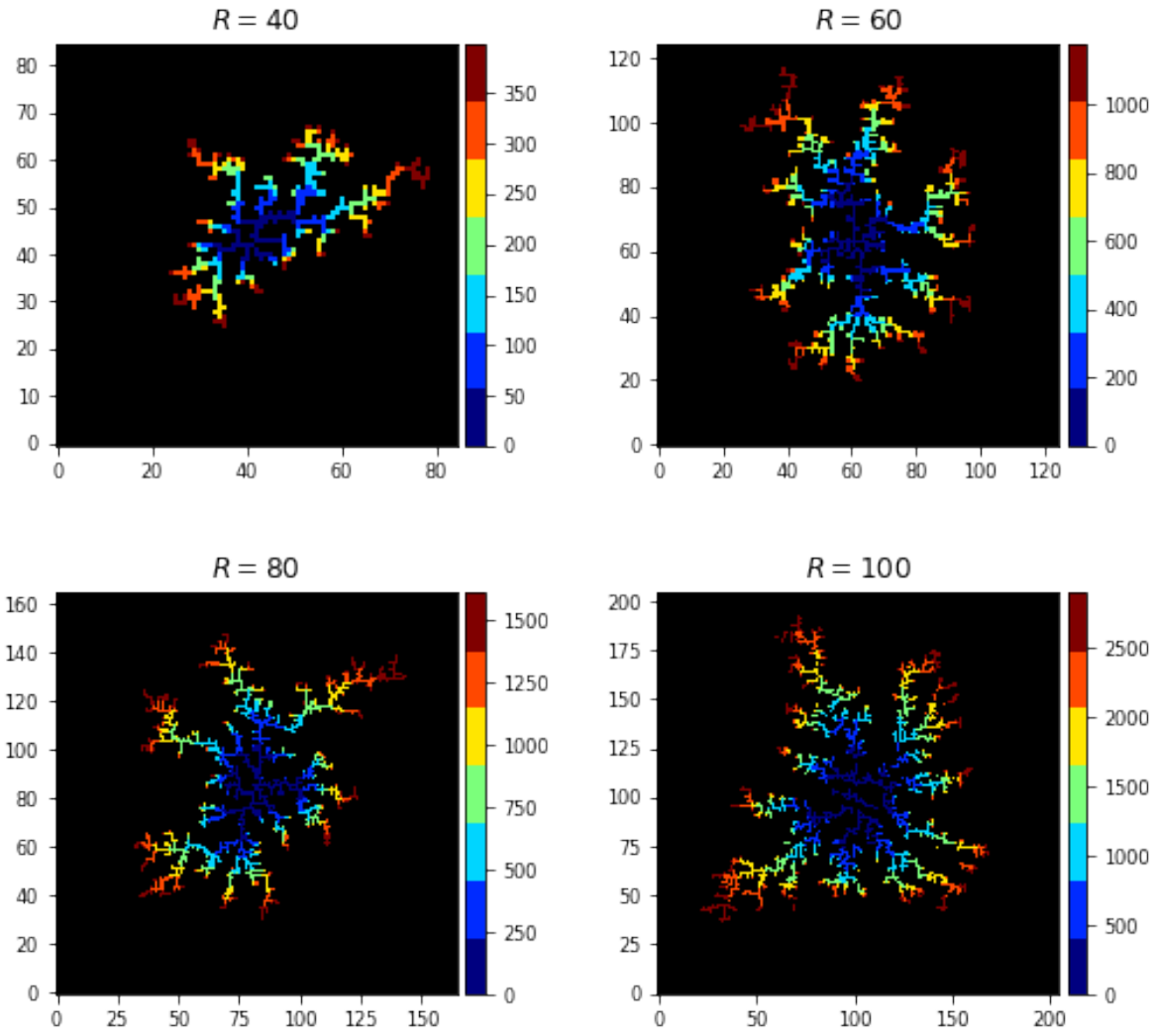

Fig. 10: DLA heatmap for a square lattice of $sl = 1$.

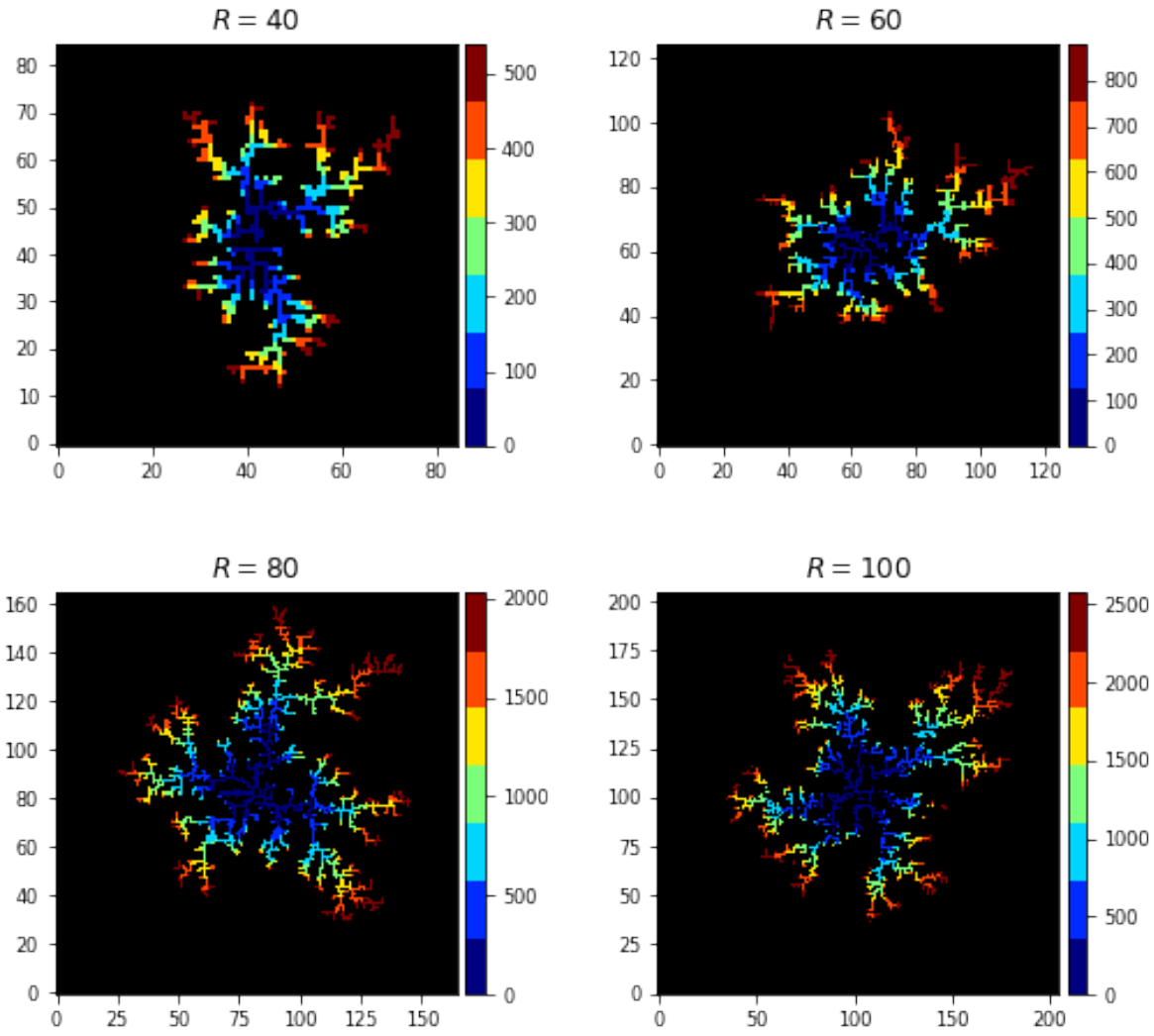

Fig. 11: DLA heatmap for a square lattice of $sl \geq 1$.

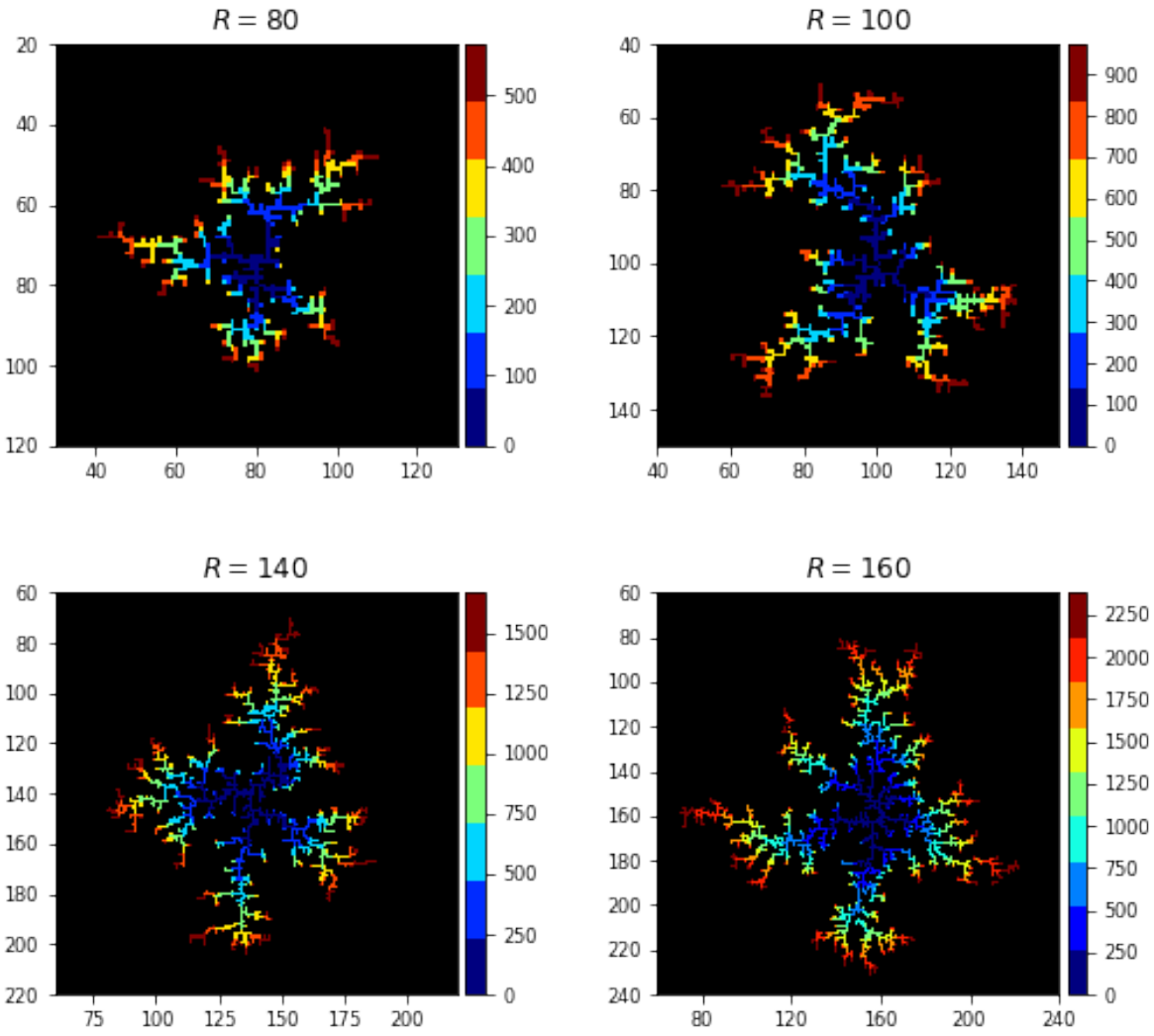

Fig. 12: DLA heatmap for a triangular lattice of $sl = 1$.